Article

Neuron

Enkephalin Disinhibits Mu Opioid Receptor-Rich Striatal Patches via Delta Opioid Receptors

Highlights

- Synaptic inhibition in patches arises from within patches but not matrix
- Enkephalin facilitates patch output through a disinhibitory mechanism
- Mu opioid receptors are expressed in both striatal pathways in patches
- Delta opioid receptors on striatopallidal neurons are the primary target of enkephalin

Authors

Matthew Ryan Banghart, Shay Quentin Neufeld, Nicole Christine Wong, Bernardo Luis Sabatini

Correspondence

Bernardo_Sabatini@hms.harvard.edu

In Brief

Opioid neuropeptides and their receptors are prominent in striatal compartments known as patches (striosomes) and matrix. We show that enkephalin facilitates cortically driven action potential firing selectively in mu opioid receptor-rich patches of the dorsal striatum through a disinhibitory mechanism that is dominated by the delta opioid receptor.

Banghart et al., 2015, Neuron *88*, 1227–1239
December 16, 2015
http://dx.doi.org/10.1016/j.neuron.2015.11.010

CellPress

Neuron
Article

Enkephalin Disinhibits Mu Opioid Receptor-Rich Striatal Patches via Delta Opioid Receptors

Matthew Ryan Banghart,[1,2] Shay Quentin Neufeld,[1,2] Nicole Christine Wong,[1] and Bernardo Luis Sabatini[1,*]
[1]Howard Hughes Medical Institute, Department of Neurobiology, Harvard Medical School, 220 Longwood Ave, Boston, MA, 02115, USA
[2]Co-first author
*Correspondence: Bernardo_Sabatini@hms.harvard.edu
http://dx.doi.org/10.1016/j.neuron.2015.11.010

SUMMARY

Opioid neuropeptides and their receptors are evolutionarily conserved neuromodulatory systems that profoundly influence behavior. In dorsal striatum, which expresses the endogenous opioid enkephalin, patches (or striosomes) are limbic-associated subcompartments enriched in mu opioid receptors. The functional implications of opioid signaling in dorsal striatum and the circuit elements in patches regulated by enkephalin are unclear. Here, we examined how patch output is modulated by enkephalin and identified the underlying circuit mechanisms. We found that patches are relatively devoid of parvalbumin-expressing interneurons and exist as self-contained inhibitory microcircuits. Enkephalin suppresses inhibition onto striatal projection neurons selectively in patches, thereby disinhibiting their firing in response to cortical input. The majority of this neuromodulation is mediated by delta, not mu-opioid, receptors, acting specifically on intra-striatal collateral axons of striatopallidal neurons. These results suggest that enkephalin gates limbic information flow in dorsal striatum, acting via a patch-specific function for delta opioid receptors.

INTRODUCTION

The striatum is the principal input nucleus of the basal ganglia, a group of brain nuclei critical for generating purposeful movements and reinforcing behaviors that maximize reward. Many aspects of basal ganglia and striatal circuitry, including neurochemical markers and projection patterns, are conserved across vertebrates (Reiner et al., 1998; Stephenson-Jones et al., 2012). In particular, the opioid peptide enkephalin (enk) is selectively expressed by striatopallidal neurons in birds, fish, and mammals, suggesting that it mediates a highly conserved function in the basal ganglia (Reiner, 2010).

Enk-expressing striatopallidal neurons, also known as indirect pathway striatal projection neurons (iSPNs), are distinct from striatonigral neurons of the direct pathway (dSPNs), which instead express dynorphin and substance P. Together, these GABAergic projection neurons comprise ~90% of all striatal neurons, are physically intermixed throughout striatum, and account for all striatal output. In rodents, cats, and primates, opioid peptide and receptor expression patterns demarcate a second, mesoscale organization of the striatum consisting of subdivisions into patch (or striosome) and matrix compartments. The patch compartment occupies 10%–20% of the striatal volume and expresses high levels of the mu opioid receptor (MOR), which is relatively absent from the surrounding matrix (Herkenham and Pert, 1981; Pert et al., 1976; Ragsdale and Graybiel, 1981). In contrast, enk, an endogenous ligand for MORs, is enriched in the matrix over patches in mice (Koshimizu et al., 2008). Since the dorsal striatum lacks beta-endorphin (Khachaturian et al., 1985), enk is likely the primary endogenous ligand for MORs in patches. Because patches exist as an interconnected tubular labyrinth coursing through the matrix (Desban et al., 1993; Graybiel and Ragsdale, 1978), enk signaling may represent a central means of communication between striatal patch and matrix compartments.

Several features of patch and matrix circuitry suggest that they operate in parallel to mediate distinct functions. First, excitatory inputs to each compartment are segregated according to cortical area, with patches preferentially innervated by limbic-associated cortical regions and matrix receiving biased innervation from sensorimotor cortices (Donoghue and Herkenham, 1986; Gerfen, 1984; Goldman-Rakic, 1982; Ragsdale and Graybiel, 1981). Second, the dendrites and local axon collaterals of SPNs conform to compartmental boundaries (Kawaguchi et al., 1989). Lastly, dSPNs in patches project directly to dopaminergic neurons in the substantia nigra pars compacta (SNc), whereas matrix dSPNs project to GABAergic neurons of basal ganglia output nuclei, the substantia nigra pars reticulate, and the endopeduncular nucleus (Fujiyama et al., 2011; Gerfen, 1984; Watabe-Uchida et al., 2012). Thus, patch and matrix compartments are proposed to operate as independent and functionally separate microcircuits with distinct inputs, local circuitry, and outputs. These anatomical relationships are consistent with the implication of patches in experience-based locomotor learning and reward-guided behavior (Canales and Graybiel, 2000; Friedman et al., 2015; Lawhorn et al., 2009; White and Hiroi, 1998).

Despite the abundance of enk in striatum and the conspicuous expression of MORs in patches, the functional consequence of enk action in patches versus matrix is not known. The sole study of opioid signaling in patches observed MOR-mediated suppression of both excitatory and inhibitory synaptic transmission

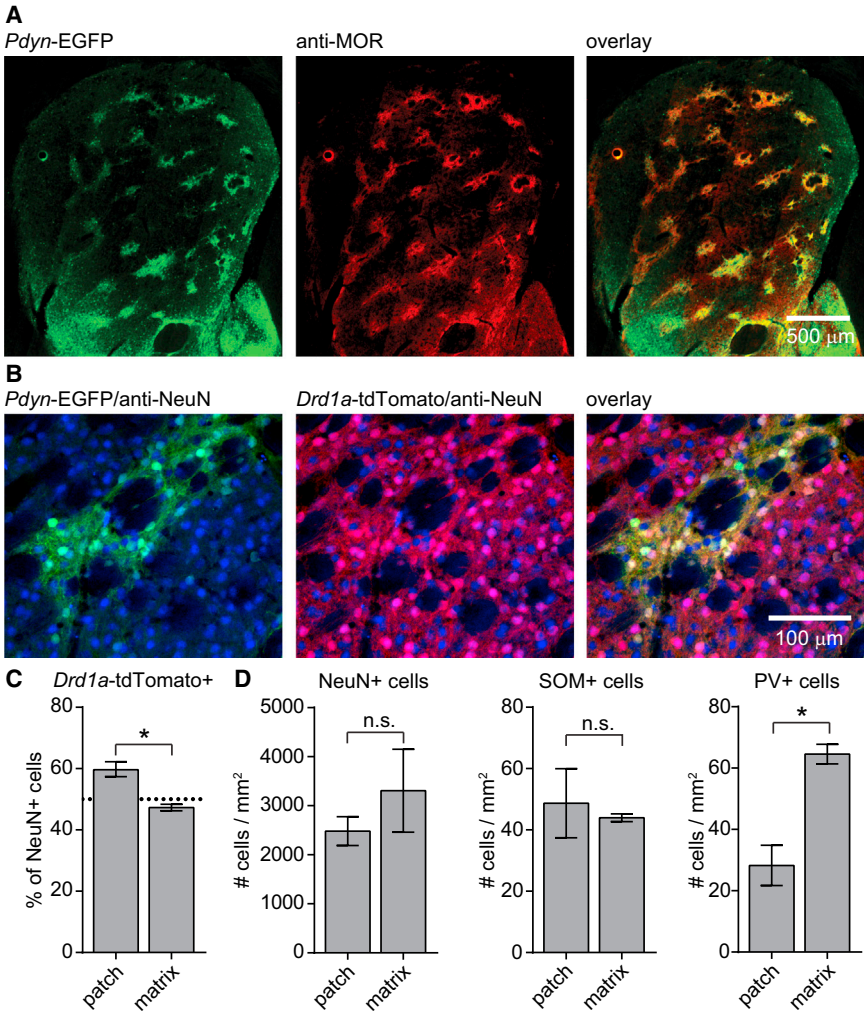

Figure 1. Visualization of Patch and Matrix Compartments in *Pdyn*-EGFP Transgenic Mice

(A) Fluorescence mosaic image of a coronal section of a *Pdyn*-EGFP (green, left) mouse immunolabeled against the MOR (red, middle). EGFP expression closely matches the distribution of MOR-rich patches (right). This mosaic image was acquired and generated on an Olympus VS120 microscope.

(B) Confocal fluorescence image of a striatal patch (green) in a coronal slice of a *Pdyn*-EGFP (green) and *Drd1a*-tdTomato (red) double transgenic mouse immunolabeled against the neuronal marker NeuN (blue). EGFP is expressed in patches only in dSPNs, which express tdTomato (right).

(C) Quantification of *Drd1a*-tdTomato+ cells in patches and matrix. The percentage of NeuN+ cells expressing tdTomato was higher in patches than in the matrix. Bars graphs indicate the mean (± SEM). *$p < 0.05$ using a two-tailed Mann-Whitney U test.

(D) Quantification of cell density in patch and matrix compartments. Cell classes were immunolabeled for identification in sections from *Pdyn*-EGFP mice. No significant difference in the density of NeuN+ cells (left) or SOM+ interneurons (middle) was observed, whereas PV+ interneurons were more abundant in the matrix. Examples of SOM and PV immunolabeling are presented in Figure S2. Bars graphs indicate the mean (± SEM). *$p < 0.05$ using a two-tailed Mann-Whitney U test.

(Miura et al., 2007). However, enk also binds delta opioid receptors (DORs), which appear to be uniformly expressed in striatum. Both MORs and DORs are $G\alpha_{i/o}$-coupled GPCRs that typically suppress cellular excitability and synaptic transmission. How the actions of enk translate into changes in circuit output depend on its cellular and synaptic targets and what their functional roles are in the microcircuit. Thus, the cumulative actions of enk in striatum remain to be determined.

In this study, we use transgenic mice that enable a priori identification of both striatal pathways (dSPN versus iSPN) and compartments (patch versus matrix) to analyze the microcircuitry and modulation of patches in mice. Using a combination of histochemical methods and targeted electrophysiological recordings in brain slices, we defined the cellular components of the patch microcircuit, revealed that enk functions in a compartment-specific manner, identified its cellular and receptor targets, and determined its net functional effect on circuit output. Our results provide a detailed understanding of the circuit mechanism by which enk selectively modulates activity in patches and provide critical insight into the functional relevance of enk signaling in dorsal striatum.

RESULTS

Patches in the Dorsal Striatum Are Isolated Microcircuits

Analysis of the structure and function of striatal patches has been hindered by the lack of tools to readily identify patches in living tissue. We took advantage of a bacterial artificial chromosome (BAC) transgenic mouse in which EGFP is expressed under the control of the promoter for prodynorphin (*Pdyn*). Throughout this study experiments were performed in the dorsal striatum (Figure S1A) of P28–P35 mice. EGFP expression in dorsal striatum of *Pdyn*-EGFP BAC transgenic mice is largely restricted to regions of neuropil immunohistochemically labeled for MORs (Figure 1A) (Cui et al., 2014; Gong et al., 2003). Using EGFP expression to identify patches, we found that they comprise 10% ± 3% of the dorsal striatal volume (Figure S1A), similar to previous estimates in several organisms (Crittenden and Graybiel, 2011).

In *Pdyn*-EGFP mice, EGFP expression is restricted to dSPNs, as revealed in mice also carrying the *Drd1a*-tdTomato BAC (Ade et al., 2011), in which red fluorescence labels all dSPNs (Figure 1B). EGFP was detected in 86% of tdTomato-expressing neurons (228 of 264 cells), and there was no coexpression of EGFP with transgenically labeled iSPNs (see Experimental Procedures; Figures S1B and S1C) or immunohistochemically identified interneuron classes (Figure S2). This high specificity and selectivity of labeling of patch dSPNs with a marker visible in

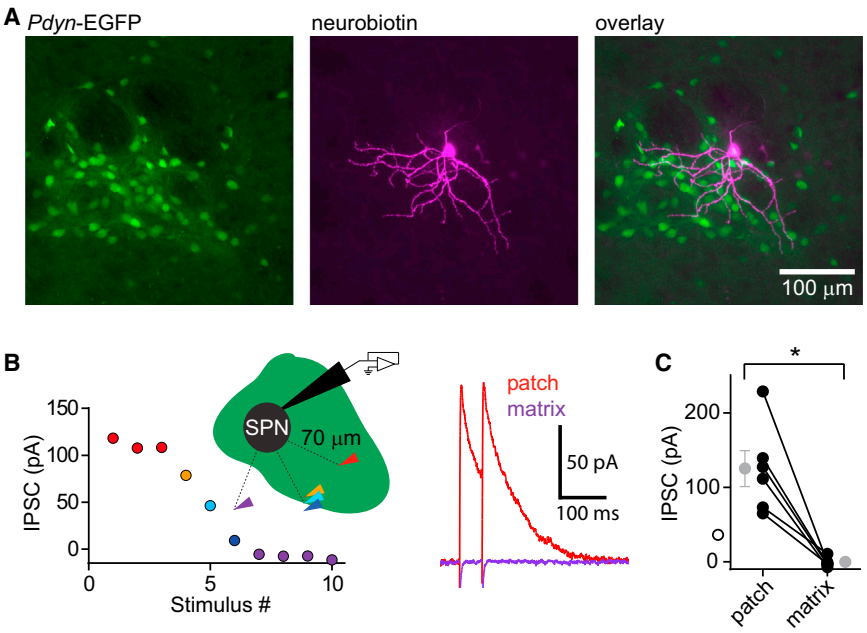

Figure 2. Anatomical and Functional Isolation of Patch and Matrix Compartments

(A) Confocal fluorescence image of a neurobiotin-filled dSPN located near the border within a patch. The dendrites of this patch SPN remained within the patch.

(B) Electrical stimulation with a small bipolar electrode reveals a lack of inter-compartmental inhibitory synaptic connectivity. Left: IPSC amplitude dropped dramatically when the stimulating electrode was moved at equal distance from the cell body into the matrix, as depicted in the schematic. Right: Representative traces (average of three trials) obtained with the electrode placed 70 μm away from the recorded cell in the patch (red) and matrix (purple).

(C) Summary plot of the IPSC amplitudes evoked in each patch neuron by stimulation in the patch and matrix shown as connected dots. Averages across cells are shown in gray (mean ± SEM). *$p < 0.05$, one-tailed Wilcoxon signed-rank test.

acute brain slices permits systematic analyses of both cellular composition and the electrophysiological properties of striatal patches. However, because *Pdyn*-EGFP incompletely labels patch dSPNs (86%), we frequently included the *Drd1a*-tdTomato transgene in order to identify all dSPNs in both compartments, and by exclusion of tdTomato, target iSPNs.

Previous anatomical analyses have reported conflicting results as to whether the cellular composition of patch and matrix compartments is distinct (Besson et al., 1990; Gerfen and Young, 1988). Immunolabeling of striatal slices from *Pdyn*-EGFP;*Drd1a*-tdTomato mice for the neuron-specific nuclear protein NeuN (Figure 1B) revealed that dSPNs are overrepresented in patches (patch: 60% ± 3% [245 of 417] NeuN+ neurons are tdTomato+; matrix: 47% ± 1% [217 of 456] NeuN+ neurons are tdTomato+; 7 images, 2 mice, $p = 0.0023$) (Figure 1C), although overall neuronal density is similar across compartments (patch: 2,483 ± 295 cells/mm^2; matrix: 3,305 ± 846 cells/mm^2; $p = 0.45$) (Figure 1D). We found no difference in the density of cells immunopositive for somatostatin (SOM) (patch: 49 ± 11 cells/mm^2, $n = 33$ cells; matrix: 44 ± 1 cells/mm^2, $n = 361$ cells; 4 images, 2 mice, $p > 0.99$) (Figure 1D). In contrast, parvalbumin (PV)-expressing cells were approximately half as abundant in patches compared to matrix (patch: 28 ± 7 cells/mm^2, $n = 27$ cells; matrix: 65 ± 3 cells/mm^2, $n = 564$ cells; 5 images, 2 mice, $p = 0.0079$) (Figure 1D). In agreement with this, synaptophysin labeling of presynaptic terminals of PV cells provided sparser innervation of patches relative to matrix (Figure S3). Together, these data indicate that patch microcircuits are enriched in dSPNs and have reduced PV cell innervation compared to the surrounding matrix.

Anatomical data suggest that patch and matrix compartments have segregated local inhibitory connectivity (Kawaguchi et al., 1989), but this has not been tested functionally. Furthermore, several interneuron classes may break this rule (Penny et al., 1988). High-magnification images of EGFP$^+$ neuronal processes and neurobiotin-filled dSPNs confirmed that dendrites originating from cells inside patches remain within patches, even if the cell body is near the compartment boundary (Figure 2A).

To examine whether SPNs within patches are functionally innervated by neurons residing in the matrix, we recorded synaptic currents in patch neurons under whole-cell voltage-clamp in acute brain slices of *Pdyn*-EGFP mice. Inhibitory synaptic transmission was evoked using small bipolar stimulating electrodes placed in the same patch compartment as the recorded cell and isolated pharmacologically by blocking glutamate receptors with NBQX and CPP. After obtaining a stable baseline, the stimulating electrode was moved stepwise into the matrix, maintaining a fixed radial distance from the soma of the recorded cell of ~70 μm (Figure 2B). At the compartment border, the evoked amplitude of the evoked inhibitory post-synaptic current (IPSC) dropped rapidly with small changes in the position of the stimulating electrode and was lost altogether in the matrix (patch: 124 ± 24 pA; matrix: −1 ± 2 pA; $n = 6$ cells, $p = 0.016$) (Figure 2C). IPSCs recovered upon moving the electrode back into the patch (not shown). Therefore, patches do not receive substantial inhibition from neurons in the surrounding matrix.

Opioid Receptors Are Expressed in SPNs of Both Pathways

Given the synaptically isolated nature of the patch compartment, communication between patch and matrix compartments might be carried out by neuromodulators, which are capable of signaling over substantial distances in tissue. Consistent with this idea, enk is expressed at higher levels in the matrix than in patches (Figure S4) (Koshimizu et al., 2008). Since patches are highly enriched in MORs, enk may signal from the matrix into patches. Alternatively, enk could also activate DORs, which are expressed throughout striatum. Despite the enrichment of

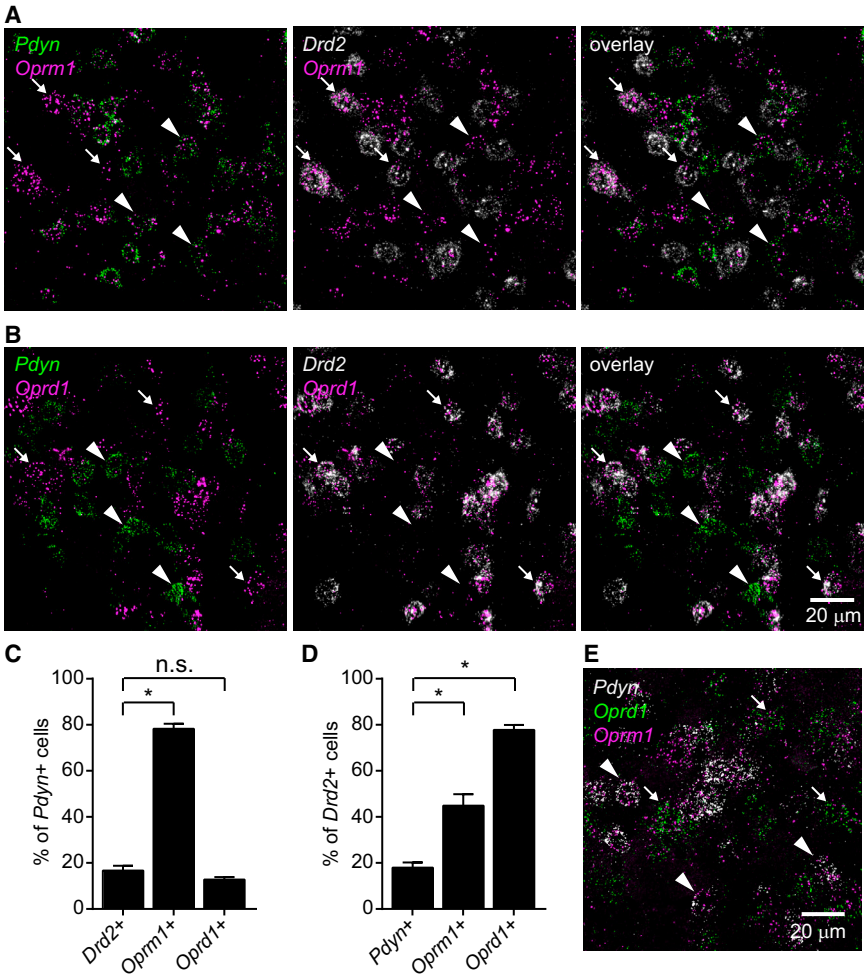

Figure 3. Opioid Receptor Distribution in SPNs as Revealed by Three-Color FISH

(A) Example of staining within a patch for Prodynorphin (*Pdyn*, green), the MOR (*Oprm1*, magenta), and the D2 dopamine receptor (*Drd2*, white). Although there is very little co-localization of *Pdyn* and *Drd2*, *Oprm1* is found with both transcripts. Large arrowheads indicate example *Pdyn*+ cells, and small arrows indicate *Drd2*+ cells. Nuclear DAPI staining is omitted for clarity.

(B) Example of staining within a patch for *Pdyn* (green), the DOR (*Oprd1*, magenta), and *Drd2* (white). *Oprd1* is only found in cells expressing *Drd2*.

(C) Quantification of the co-expression of *Drd2*, *Oprm1*, and *Oprd1* with *Pdyn*. Bars represent the mean (+SEM) percentage of *Pdyn*+ DAPI-stained nuclei also expressing the indicated transcripts. *$p < 0.05$ using a two-tailed Mann-Whitney U test. *Oprm1*, but not *Oprd1*, is found in cells expressing *Pdyn*.

(D) Quantification of the co-expression of *Pdyn*, *Oprm1*, and *Oprd1* with *Drd2*. Bars represent the mean percentage (+SEM) of *Drd2*+ DAPI-stained nuclei also expressing the indicated transcripts. Both *Oprm1* and *Oprd1* are found in cells expressing *Drd2*.

(E) Example of staining within a patch for *Pdyn* (white), *Oprd1* (green), and *Oprm1* (magenta). *Oprm1* and *Oprd1* are co-expressed but only in *Pdyn*− cells. Large arrowheads indicate example *Pdyn*+ cells, and small arrows indicate example *Oprd1*+ cells. Summary data for (E) is presented in Figure S6C.

MORs in patches and demonstration of their expression in dSPNs (Cui et al., 2014), which cells within the striatum express DORs and MORs remains unclear.

Neuron classes that express MORs and DORs were identified by fluorescence in situ hybridization (FISH) to examine the expression of multiple mRNAs in individual cells. dSPNs and patches were identified by labeling for *Pdyn*, and iSPNs were distinguished by the labeling for *Drd2*. Although strongly negatively correlated (Figure S5), we observed co-labeling of *Pdyn* and *Drd2* probes in 17%–18% of cells in patches (see Supplemental Experimental Procedures). Given the lack of co-labeling of iSPNs and dSPNs with transgenic markers, this value likely estimates the false-positive co-expression rate. We therefore used the co-labeling of *Pdyn* and *Drd2* as a control for evaluating opioid receptor expression in each cell class.

We quantified the number of fluorescent puncta corresponding to transcripts for *Oprm1* (encoding MORs) or *Oprd1* (encoding DORs) in dSPNs and iSPNs in both patches and matrix (Figures 3A, 3B, and S5). Consistent with the prominence of MOR protein in patches, *Oprm1* was detected in a greater percentage of cells located within *Pdyn*-enriched patches than in the matrix (Figure S6A). Furthermore, the number of transcripts per cell was greater in patches than in matrix (Figure S6B). In contrast, *Oprd1* was detected uniformly in both compartments, both in terms of the percentage of *Oprd1*+ cells and the number of transcripts per cell (Figures S6A and S6B), consistent with prior studies using radiolabeled ligands that bind DORs (for example, Pradhan and Clarke, 2005).

Within patches most *Pdyn*+ dSPNs expressed *Oprm1*, but not *Oprd1* (*Oprm1*+: 78% ± 2%, n = 1622 cells, 5 images, 3 mice, $p = 0.0010$; *Oprd1*+: 13% ± 1%, n = 1,003 cells, 4 images, 2 mice, $p = 0.19$) (Figure 3C). In contrast, most *Drd2*+ iSPNs expressed *Oprd1* and only about half expressed *Oprm1* (*Oprd1*+: 78% ± 2%, n = 1,003 cells, 4 images, 2 mice, $p = 0.0028$; *Oprm1*+: 45% ± 5%, n = 1,622 cells, 5 images, 3 mice, $p = 0.0010$) (Figure 3D). These data suggest that individual iSPNs might express both DOR and MOR in patches. Indeed, in a separate experiment, we confirmed co-expression of *Oprm1* and *Oprd1* in patch iSPNs using triple FISH for *PDyn*, *Oprm1*, and *Oprd1* (Figure 3E). The vast majority of cells expressing both *Oprm1* and *Oprd1* were negative for *Pdyn* (Figure S6C). Therefore, these results (tabulated in Figure S6D) suggest that the potential GPCR targets for enk in patches are MORs and DORs on iSPNs and MORs on dSPNs.

Enkephalin Suppresses Synaptic Inhibition in Patches but Not Matrix

The observation that SPNs in patches express opioid receptors raises the possibility that enk might alter the membrane excitability of both dSPNs and iSPNs. To test for this, we expressed channelrhodopsin-2 (ChR2) (Boyden et al., 2005) in SPNs and applied enk during cell-attached recordings from ChR2-expressing neurons in order to preserve cytosolic signaling molecules that may be downstream of opioid receptors. ChR2 was selectively expressed in dSPNs or iSPNs by infection with Cre-dependent adeno-associated virus (AAV) in the appropriate transgenic animal. In the presence of a cocktail of antagonists for ionotropic and metabotropic glutamate and GABA receptors, ramps of blue light evoked trains of action potentials that progressively increased in frequency (Figure 4A). To sensitively detect changes in excitability, light intensities were chosen to trigger spike trains that exhibit minimal accommodation, which typically involved a 1-s delay to the first spike and maximal instantaneous firing rates of 30–40 Hz. After achieving stable responses, enk (leucine-enkephalin) was applied by bath perfusion at a concentration that strongly activates MORs and DORs (30 μM). The number of light-evoked action potentials evoked per trial was unaffected by 3–5 min of enk application (dSPNs: 95% ± 10% of baseline, n = 9 cells, p = 0.44; iSPNs: 100% ± 3% of baseline, n = 6 cells, p > 0.99; p values reflect comparison of enk to baseline, see Experimental Procedures) (Figure 4B). Thus, despite the expression of opioid receptors by SPNs, enk does not directly regulate the excitability of dSPNs or iSPNs in patches.

It is well established that MOR and DOR agonists suppress excitatory transmission onto SPNs by 10%–30% in both patches and matrix (Atwood et al., 2014; Blomeley and Bracci, 2011; Jiang and North, 1992; Miura et al., 2007). We therefore focused on inhibitory synaptic transmission. In acute brain slices prepared from *Pdyn*-EGFP;*Drd1*-tdTomato mice, we obtained whole-cell voltage-clamp recordings from identified dSPNs and iSPNs located in both patches and matrix. IPSCs were evoked electrically in the presence of NBQX and CPP (Figure 4C), as well as the muscarinic antagonist scopolamine to prevent potential confounds due to modulation of enk-sensitive cholinergic neurons (Jiang and North, 1992; Ponterio et al., 2013). Example IPSCs recorded from SPNs in the matrix and patches are shown in Figure 4D, before and 3–5 min after enk application. For each neuron, the effect on IPSC amplitude was calculated as follows:

$$\Delta IPSC = 100 \cdot (\Delta IPSC_{enk} - \Delta IPSC_{baseline}) / \Delta IPSC_{baseline}.$$

IPSCs recorded from dSPNs in the matrix were insensitive to enk but in patches they were strongly suppressed (matrix: $\Delta IPSC$ = 6% ± 8%, n = 11, p = 0.64; patch: −54% ± 4%, n = 19, p < 0.00010) (Figures 4E and 4F). Similar actions were observed with methionine-enkephalin, another enkephalin analog abundant in striatum, as well as with a lower concentration of enk (1 μM) indicating that 30 μM saturates striatal opioid receptors (Figure S7B). IPSCs recorded from iSPNs were also insensitive to enk in matrix and significantly suppressed in patches (matrix: 3% ± 8%, n = 6, p = 0.84; patch: −36% ± 4%, n = 8, p = 0.0078) (Figure S7C), although to a lesser extent compared to dSPNs (p = 0.0013, Figure 4F). Therefore, suppression of inhibition by enk is robust and specific to patches. Because inhibition onto dSPNs was more sensitive to enk, and due to their potential to influence dopamine signaling in the striatum, we focused on recordings from patch dSPNs for all subsequent studies.

Suppression of inhibition by enk was completely blocked in the presence of opioid antagonists ($\Delta IPSC$ = −2% ± 2%, n = 5, Figure 4G). To determine whether this suppression is transient or a form of long-term plasticity, we chased enk from the bath with opioid antagonists (Figure 4H). Within 5–10 min of washout, we observed near complete recovery of the IPSC (−61% ± 11% in enk versus −6% ± 7% after washout, n = 5 cells, p = 0.031). Therefore, suppression of inhibition by enk is an acute, reversible modulation. The locus of modulation could be either pre- or post-synaptic, since SPNs of both pathways express opioid receptors. We were unable to obtain positive evidence for modulation of either the pre- or post-synaptic terminal, as enk application did not significantly alter paired-pulse ratios, spontaneous miniature IPSC (mIPSC) amplitude or frequency, or GABA uncaging-evoked currents (Figures S7D–S7G).

DORs Are the Major Receptor Target of Enkephalin in Patches

To determine if activation of MOR mediates the actions of enk, we examined suppression of inhibition in *Pdyn*-EGFP;*Oprm1*$^{-/-}$ mice (Matthes et al., 1996). In these mice, which lack MORs but retain patches (Figure 5A), enk application still strongly suppressed IPSC amplitude ($\Delta IPSC$ = −46% ± 7%, n = 8 cells, p = 0.0039) (Figures 5B and 5C). Similarly, in *Pdyn*-EGFP;*Oprd1*$^{-/-}$ mice (Filliol et al., 2000) patches were retained (Figure 5A) and inhibition was also suppressed, albeit to a lesser extent than either wild-type or *Oprm1*$^{-/-}$ conditions ($\Delta IPSC$ = −28% ± 5%, n = 10 cells, p = 0.0019) (Figures 5B and 5C). These results indicate that neither receptor is strictly necessary for enk to suppress inhibition and suggest a contribution from both MORs and DORs.

In order to assess whether either MOR or DOR activation is sufficient to explain the effects of enk, we selectively activated each receptor pharmacologically. SNC-80 exhibits >10,000× selectivity for DORs over MORs (Knapp et al., 1996), allowing selective activation of DORs in brain slices. Although DAMGO is the prototypical MOR-selective agonist, we found that DAMGO application reduced inhibition in *Pdyn-EGFP;Oprm1*$^{-/-}$ mice when applied at 1 μM but not 300 nM (Figures S8A and S8B). The effects of 1 μM DAMGO in the *Pdyn*-EGFP;*Oprm1*$^{-/-}$ mice were blocked by the highly selective DOR antagonist TIPP-Psi (3 μM, Figures S8A and S8B), at a concentration we independently verified to exhibit selectivity for DORs (Figures S8C and S8D). We therefore used 300 nM DAMGO in the presence of 3 μM TIPP-Psi to selectively probe MORs. Under this stringent condition, DAMGO application suppressed inhibition by 22% ± 4% (n = 9 cells, p = 0.0019), confirming that MOR activation is sufficient to suppress inhibition (Figure 5C). DOR agonism by SNC-80 (500 nM), however, produced an approximately 2-fold larger effect ($\Delta IPSC$ = −41 ± 8%, n = 11 cells, p = 0.0010) (SNC-80 versus DAMGO, p = 0.032), which was blocked by 3 μM TIPP-Psi (Figure S8E). Consistent with additive contributions

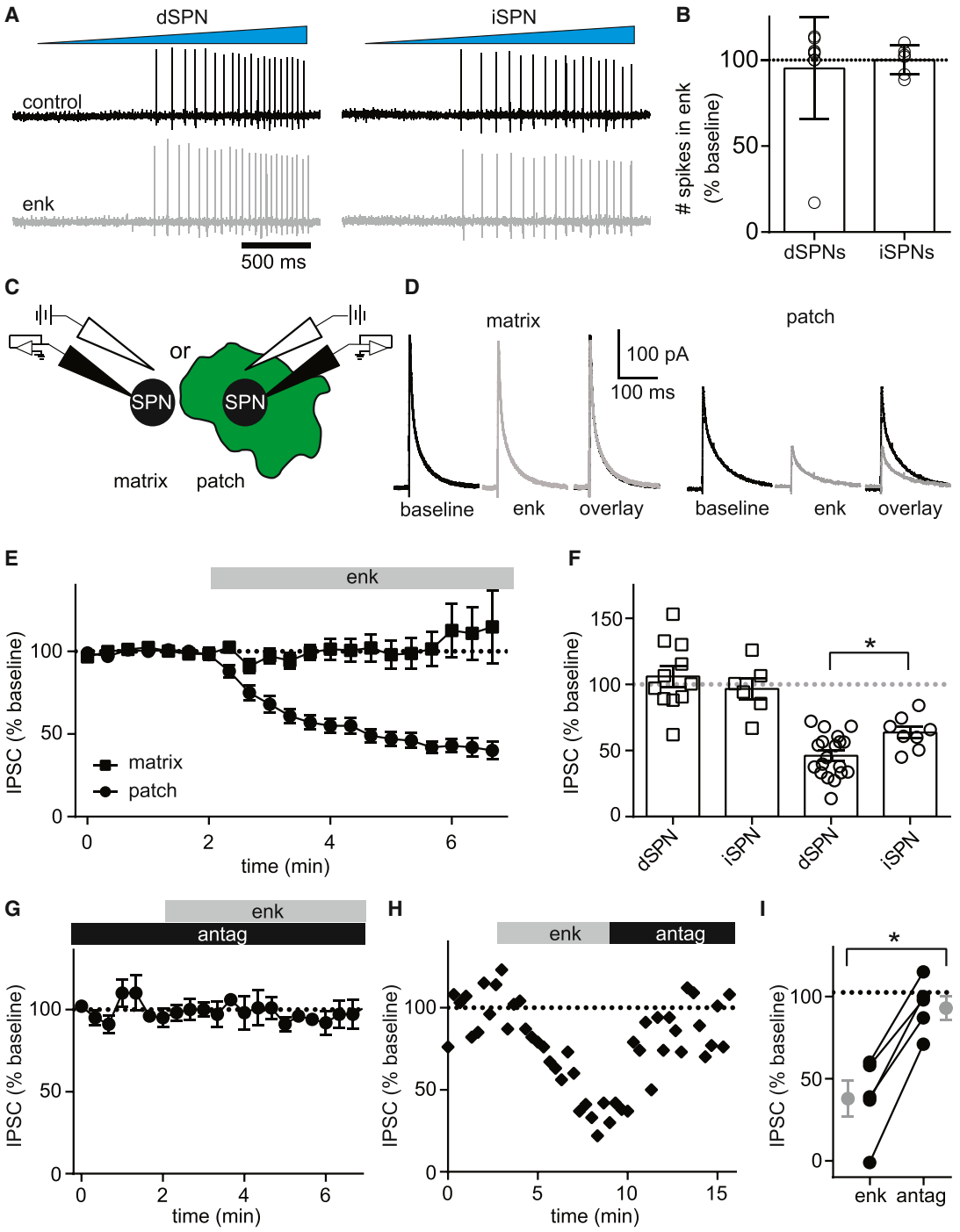

Figure 4. Enkephalin Suppresses Inhibition onto dSPNs and iSPNs in Patches but Not Matrix

(A) Cell-attached recordings of action potential firing from a dSPN (left) and iSPN (right) in the absence (top) and presence (bottom) of enk (30 μM), evoked by a 2-s, 473-nm blue light ramp. Action potential firing is unchanged by enk. ChR2 was targeted to dSPNs or iSPNs using the following transgenic animals: *Drd1a*-Cre;*Pdyn*-EGFP for dSPNs; *Adora2A*-Cre;*Pdyn*-EGFP for iSPNs; and *Dlg3*-Cre;*Drd1a*-tdTomato;Ai32 for either (see Figure S7A).

(B) Summary data showing average number of spikes per trial evoked during the 2-s stimulus in the presence of enk normalized to baseline. Averages from each cell are shown as open circles. The superimposed bars indicate the mean (± SD).

(C) Schematic illustrating the experimental configuration. Whole-cell voltage-clamp recordings of dSPNs or iSPNs were obtained in the patch or matrix compartments in acute brain slices from *Pdyn*-EGFP;*Drd1a*-tdTomato mice. Glass stimulating electrodes were placed in the same compartment within 100 μm of the recorded cell.

(legend continued on next page)

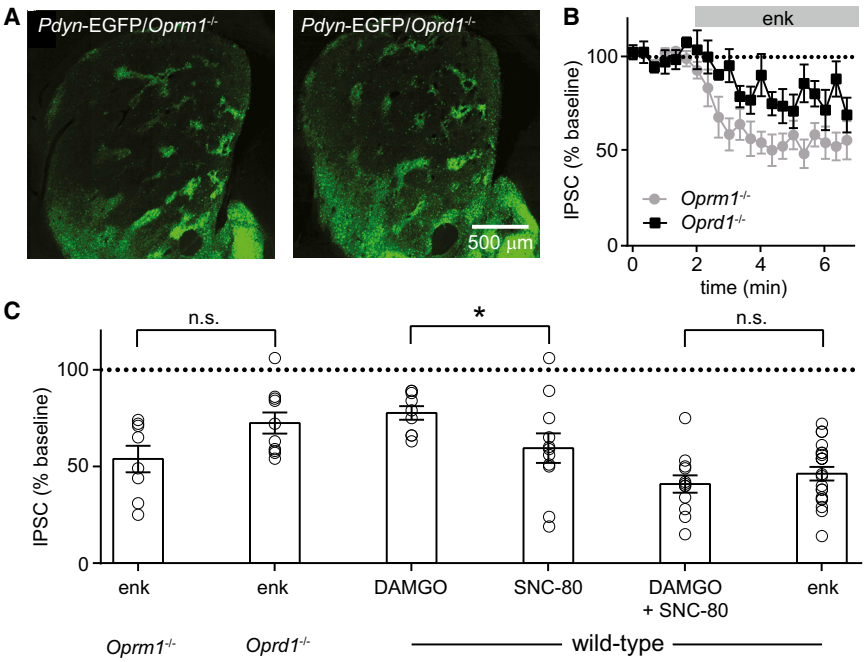

Figure 5. DORs, Not MORs, Dominate the Suppression of Inhibition by Enkephalin

(A) Fluorescence mosaic images of EGFP expression in coronal sections taken from *Pdyn*-EGFP;*Oprm1*$^{-/-}$ (left) and *Pdyn*-EGFP;*Oprd1*$^{-/-}$ (right) mice. In both cases, patches are present and do not display gross abnormalities. Mosaic images were acquired and generated on an Olympus VS120 microscope.

(B) Average normalized IPSC amplitudes (± SEM) over time during enk application for neurons from *Pdyn*-EGFP;*Oprm1*$^{-/-}$ (gray) and *Pdyn*-EGFP/*Oprd1*$^{-/-}$ (black) mice. In both cases IPSCs were suppressed by enk.

(C) Summary plot of the normalized average IPSCs in enk measured in *Pdyn*-EGFP;*Oprm1*$^{-/-}$ and *Pdyn*-EGFP;*Oprd1*$^{-/-}$ mice as well as in wild-type *Pdyn*-EGFP mice in the presence of the MOR agonist DAMGO, the DOR agonist SNC-80, the two combined, or enk (from Figure 4F). Although both DAMGO and SNC-80 significantly suppressed IPSCs, SNC-80 had a larger effect. The actions of co-applied SNC-80 and DAMGO were similar to enk. Averages from each cell are shown as open circles. The superimposed bars indicate the mean (± SEM). *p < 0.05 using a two-tailed Mann-Whitney U test.

from both DORs and MORs, following DOR activation with SNC-80, addition of DAMGO (1 µM) further suppressed inhibition (−59% ± 4%, n = 12 cells, p = 0.00025), to an extent indistinguishable from enk (p = 0.39). These results indicate that enk suppresses inhibition onto patch dSPNs predominately via DORs, with a smaller contribution from MORs.

iSPN Inputs to dSPNs Are the Major Cellular Target of Enkephalin in Patches

Patch SPNs receive inhibitory inputs from multiple classes of neurons, including other SPNs and GABAergic interneurons, any of which might be modulated by enk. To identify the inhibitory inputs to dSPNs that are sensitive to enk, we bred mice that express *Pdyn*-EGFP along with Cre recombinase in specific striatal cell classes. We used Cre-dependent AAVs to express ChR2 in Cre-expressing neurons and examined the effect of enk on ChR2-evoked IPSCs. We were unable to reliably evoke IPSCs in patches using two strains of mice expressing Cre under PV promoters (*Pvalb*-IRES-Cre, *Pvalb*-2A-CreERT2-D, not shown), possibly due to the relative lack of innervation of patches by fast-spiking interneurons (Figures 1 and S3).

GABAergic synaptic currents were pharmacologically isolated and optogenetically evoked using blue light flashes. GABAergic IPSCs from SOM cells were not suppressed by enk (*ΔIPSC* = 4% ± 3%, n = 8 cells, p = 0.35). Inputs from dSPNs and iSPNs were suppressed by enk (dSPNs: −32% ± 8%, n = 12 cells, p = 0.0010; iSPNs: −68% ± 5%, n = 10 cells, p = 0.0020), with iSPN inputs responding more strongly than dSPN inputs (p = 0.0032) (Figures 6A–6C).

The FISH analysis indicated that MORs are present in both dSPNs and iSPNs and that DORs are exclusively expressed in iSPNs. We hypothesized that suppression of iSPN inputs onto dSPNs is mediated by DORs and possibly MORs, whereas that of dSPN inputs onto dSPNs is mediated by MORs alone. To test this, we examined each class of inputs using the selective agonists described previously (Figure 5). Consistent with the FISH findings, DAMGO slightly suppressed inhibition from both dSPN and iSPN inputs (dSPNs: −27% ± 5%, n = 10 cells, p = 0.0010; iSPNs: −17% ± 5%, n = 10 cells, p = 0.0059) (Figure 6). In contrast, SNC-80 had no effect on dSPN inputs but strongly suppressed iSPN inputs (dSPNs: −6% ± 3%, n = 11 cells, p = 0.07; iSPNs: −48 ± 7%, n = 6 cells, p = 0.016). Supporting the

(D) Example of electrically evoked IPSCs recorded in the matrix (left) or patch (right) before (black) and after (gray) application of enk. Single trial examples are shown.

(E) Average normalized IPSC amplitude (± SEM) over time during enk application for dSPNs in the matrix (squares) and patch (circles) compartments. IPSCs were strongly suppressed in patches but not matrix. For iSPNs, see Figure S7C.

(F) Summary data showing average baseline normalized IPSCs measured in the presence of enk. Averages from individual cells are shown as open squares (matrix) and circles (patch). The superimposed bars indicate the mean ± SEM. *p < 0.05 using a two-tailed Mann-Whitney U test.

(G) Average normalized IPSC amplitudes (± SEM) over time for dSPNs in patches during enk application in the presence of an opioid antagonist cocktail (3 µM naloxone; 3 µM SDM25N). Enk did not suppress inhibition in the presence of opioid antagonists.

(H) Example recording from a dSPN showing that the enk effect was reversed with an opioid antagonist cocktail (3 µM naloxone; 3 µM SDM25N).

(I) Summary plot of the baseline-normalized average IPSCs evoked in dSPNs in the presence of enk and after reversal with opioid antagonists. The averages (± SEM) for individual neurons are shown as connected dots and across cells in gray. *p < 0.05, one-tailed Wilcoxon signed-rank test.

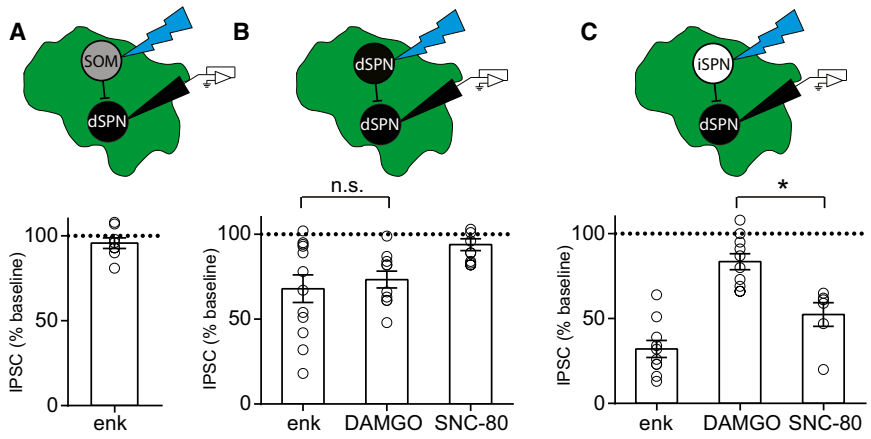

Figure 6. Optogenetic Activation of Striatal Cell Classes Reveals that Inhibition Arising from dSPNs and iSPNs Is Suppressed by Enkephalin in Patches

(A) Synaptic inhibition originating from SOM interneurons is not suppressed by enk. Top: Schematic depicting selective optogenetic activation of SOM interneurons in *Sst*-Cre;*Pdyn*-EGFP mice during whole-cell voltage-clamp recordings from dSPNs in patches. Bottom: Summary plot of the normalized average IPSCs measured in enk. Throughout this figure, averages from each cell are shown as open circles. The superimposed bars indicate the mean (± SEM).

(B) Synaptic inhibition originating from dSPNs is suppressed by enk and DAMGO, but not SNC-80. Top: Schematic depicting selective optogenetic activation of dSPNs in *Drd1a*-Cre;*Pdyn*-EGFP mice during whole-cell voltage-clamp recordings from dSPNs in patches. Bottom: Summary plot of the normalized average IPSC measured in enk, DAMGO, and SNC-80.

(C) Synaptic inhibition originating from iSPNs is suppressed by enk, DAMGO, and SNC-80. Top: Schematic depicting selective optogenetic activation of iSPNs in *Adora2A*-Cre;*Pdyn*-EGFP mice during whole-cell voltage-clamp recordings from dSPNs in patches. Bottom: Summary plot of the normalized average IPSC measured in enk, DAMGO, and SNC-80. SNC-80 had a significantly greater effect than DAMGO. *$p < 0.05$ using a two-tailed Mann-Whitney U test.

lack of DORs in dSPNs, the action of DAMGO on dSPN inputs was sufficient to account for the action of enk ($p = 0.91$). This was not the case for suppression of iSPN input, where SNC-80 dominated the effect over DAMGO (SNC-80 versus DAMGO, $p = 2.0 \times 10^{-4}$). These data support a local circuit model in which enk suppresses inhibition onto dSPNs predominantly via DORs on iSPN inputs, and to a lesser extent via MORs influencing both iSPN and dSPN inputs.

Enkephalin Disinhibits Patch dSPNs

Given that enk does not directly modulate SPN firing but strongly reduces SPN to SPN collateral inhibition, we hypothesized that the net outcome of enk signaling in patches is disinhibition during prolonged excitatory drive. To investigate this possibility, we stimulated network activity by optogenetically driving cortico-striatal excitatory inputs and measured the actions of enk on SPN output (Figure 7A). Whole-cell voltage-clamp recordings revealed IPSCs at the reversal potential for glutamatergic transmission, which were strongly suppressed by enk ($\Delta IPSC = -57\% \pm 5\%$, n = 6 cells, $p = 0.016$) to a degree similar to that measured using electrical stimulation locally in patches ($p = 0.72$) (Figures 7B and 7C). Confirming that this inhibition was indeed mediated by excitatory transmission-driven disynaptic inhibition, NBQX and CPP eliminated the IPSC (reduced to 6% ± 2% of baseline, n = 6 cells, $p = 0.016$, Figures 7B and 7C).

Because opioids have been reported to reduce glutamate release in both patches and matrix (Atwood et al., 2014; Jiang and North, 1992; Miura et al., 2007), suppression of excitation might counteract suppression of inhibition and prevent the predicted facilitation of spiking in patches by enk. Therefore, we measured the consequence of enk application on action potential firing induced by cortico-striatal activation. Whole-cell current-clamp recordings from dSPNs in patches were used to monitor the responses to five blue light flashes delivered at 20–25 Hz. This stimulus typically elicited a single spike in response to the first flash, which was followed by subthreshold EPSPs (Figure 7D). On average, the number of action potentials per trial increased 3–5 min after enk application (1.11 ± 0.07 spikes during baseline versus 1.94 ± 0.36 in enk, n = 6 cells, $p = 0.031$). When discernable, the amplitude of a superimposed feedback IPSP, presumably arising from adjacent SPNs that also fired in response to cortico-striatal stimulation, also decreased (Figure 7E). In contrast, enk did not change the response of dSPNs located in the matrix to the same stimulus (1.03 ± 0.03 spikes during baseline versus 0.95 ± 0.12 in enk, n = 5 cells, $p = 0.75$, Figure 7F), consistent with selective suppression of inhibition in patches. Therefore, the net consequence of enk on striatal output is disinhibition of dSPNs in patches, enabling these neurons to better follow trains of excitatory drive from cortex. This disinhibition is specific to patches and thus represents a mechanism for opioid action to shift the balance of activity between striatal compartments to favor patches.

DISCUSSION

In this study, we used *Pdyn*-EGFP mice to identify patches and dSPNs in dorsal striatum. Our observations in mice reveal distinct microcircuitry in patches and provide functional evidence for compartmentalized synaptic transmission. We further examined the actions of the endogenous opioid neuropeptide enk on synaptic transmission and microcircuit output. Our anatomical and functional data concordantly confirm that MORs are prominent in dSPNs and that they mediate compartment-specific suppression of inhibition in patches. Surprisingly, our studies uncovered a major role for DORs in the compartmentalized actions of enk, despite their uniform expression in striatum. We pinpointed iSPNs as the major cellular target of enk predominately via its activation of DORs, and to a lesser extent via activation of MORs. We further demonstrated that this disinhibitory pathway leads to a net increase in dSPN firing in patches, highlighting the importance of DOR and inhibitory collaterals in

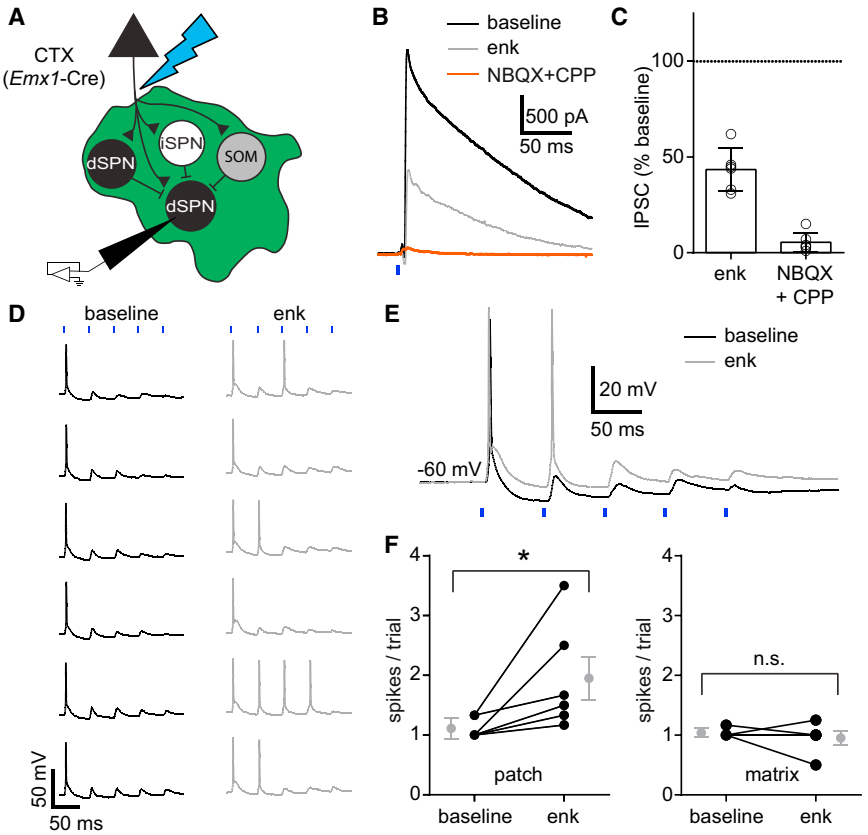

Figure 7. Enkephalin Disinhibits dSPNs in Patches

(A) Schematic depicting optogenetic activation of the striatal microcircuit in brain slice by driving corticostriatal inputs in *Emx1*-Cre;*Pdyn*-EGFP;*Drd1a*-tdTomato;Ai34 mice.

(B) Disynaptic inhibition in patches is suppressed by enk. Example IPSCs in the absence (baseline, black) and presence of enk (gray), and after the addition of NBQX and CPP (orange) to block excitatory transmission.

(C) Summary plot of the normalized average IPSC measured in enk and NBQX+CPP. Averages from each cell are shown as open circles. The superimposed bars indicate the mean (± SEM).

(D) Synaptically driven action potentials are facilitated by enk. Example current-clamp recording from a patch dSPN that was stimulated by five blue light flashes (20 Hz) before (black) and after (gray) enk application. Data were acquired every 20 s.

(E) Superimposed single-trial example responses to the blue light stimulus before (black) and after (gray) enk application. In this example, suppression of the co-incident IPSP by enk can be observed.

(F) dSPNs are disinhibited in the patch, but not matrix compartment. Summary plots of the average number of spikes per trial during the baseline period and after enk application, recorded from cells located in the patch (left) and matrix (right) compartments. The averages (± SEM) for individual neurons are shown as connected dots and across cells in gray. *$p < 0.05$, two-tailed Wilcoxon signed-rank test.

shaping cortically driven striatal output. These findings are graphically summarized in Figure 8.

Patch Microcircuitry

We characterized the circuitry of patches and conducted experiments that functionally probe synaptic compartmentalization. We found that cellular composition differs between patches and matrix with the former having higher dSPN density and a conspicuous under-representation of PV+ interneurons. Furthermore, using several transgenic mouse lines, we were unable to reliably obtain synaptic responses in patch SPNs following stimulation of PV+ interneurons, suggesting a lack of PV innervation of patch SPNs. The functional implications of this difference require further investigation.

SPN axon collaterals have been reconstructed and shown to respect compartmental boundaries (Kawaguchi et al., 1989; Penny et al., 1988). In contrast, SOM and PV interneurons seem to localize near the borders, with their axons (SOM) (Rushlow et al., 1996) and dendrites (PV) (Cowan et al., 1990; Kubota and Kawaguchi, 1993) innervating both patches and matrix. However, our results indicate that the vast majority of synaptic inhibition in patches arises from within the compartment. These results also suggest that axons of other inhibitory neurons, such as pallidostriatal projections and axons of SPNs leading out of striatum, do not generally cross patch/matrix boundaries.

Opioid Regulation of Inhibition in Patches

To understand the consequences of enk signaling, we systematically identified sites of enk action in the patch microcircuit. The intrinsic excitability of neither dSPNs nor iSPNs was sensitive to enk, despite their high expression of opioid receptors. As expected, we observed patch-specific suppression of inhibition, but unlike prior studies (Miura et al., 2007), we found that primarily DORs rather than MORs mediate this opioid effect.

The observed pathway distribution of opioid receptors in dSPNs and iSPNs in patches provides insights inaccessible in prior anatomical (Cui et al., 2014; Guttenberg et al., 1996; Oude Ophuis et al., 2014) and biochemical (Lindskog et al., 1999; Noble and Cox, 1995) studies that did not distinguish between compartments. While these studies established a clear association between MORs in dSPNs and DORs in iSPNs, they did not report evidence of MORs in iSPNs, presumably due to oversampling of SPNs in the more prominent matrix compartment. By targeting patches for analysis, we observed co-expression of MORs and DORs in iSPNs and verified this functionally. This result highlights that classic models of striatal pathway differences are not generally applicable to patches and requires that patch iSPNs be considered in future studies concerning MOR function in the striatum. Mapping the opioid receptors to dSPNs and iSPNs also provided further insight into the functional site of action of enk. The selective expression of DORs in iSPNs indicates a presynaptic site of action, although the

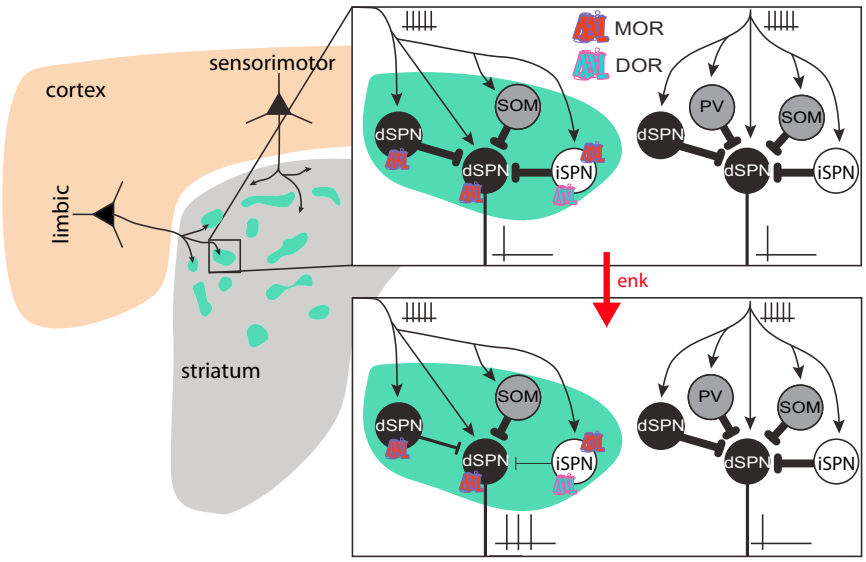

Figure 8. Summary Model of Enkephalin Modulation of the Patch Microcircuit

Patches and matrix receive different cortical inputs and locally process information with different contributions from PV interneurons. Local inhibition suppresses repetitive, high-frequency firing in response to cortical drive. By reducing inhibition from SPN collaterals via activation of MORs on dSPNs and iSPNs and DORs on iSPNs, enkephalin facilitates information flow through patches, but not matrix.

electrophysiological data presented do not conclusively support either a pre- or post-synaptic mechanism. Because MORs are expressed in both pathways, similar inferences cannot be made and the site of action of this receptor remains to be determined.

One major question that emerges from our study is how DOR-mediated modulation of inhibition is restricted to iSPN collaterals in patches. Analysis by FISH clearly demonstrates uniform expression of DORs throughout the striatum, with neither the number of *Oprd1*+ cells nor the number of transcripts expressed in each cell being different between compartments. All prior anatomical studies using radiolabeled DOR ligands also report a uniform distribution. Yet in the matrix we observed no suppression of electrically evoked inhibition or facilitation of spiking in response to cortical drive in the presence of enk (but see Jiang and North, 1992; Miura et al., 2007). The cellular mechanism underlying this compartmental specificity requires further investigation.

We and others have noted relatively low expression levels of enk in patches in comparison to matrix in mice (Figure S4) (Graybiel and Chesselet, 1984; Koshimizu et al., 2008; Tajima and Fukuda, 2013). Although this distribution supports a role for enk in intercompartmental communication, it is possible that dynorphin, a kappa opioid receptor agonist that can activate MOR and DOR with substantial potency (Pennock and Hentges, 2014; Toll et al., 1998; Zhang et al., 1998), serves as a local ligand in patches. Additionally, prodynorphin contains a copy of leu-enk. However, the vast majority of dynorphin appears to be transported out of striatum to axonal release sites in the substantia nigra (Besson et al., 1990; Chesselet and Graybiel, 1983; Fallon and Ciofi, 1990). Nonetheless, it is possible that enk and dynorphin both disinhibit patch SPNs via inter- and intra-compartmental signaling.

Implications for Striatum-Dependent Behavior

The anatomical evidence that patch dSPNs provide direct input to SNc dopamine neurons suggests that patches are uniquely positioned to control dopamine release in striatum. Our findings imply that enk could indirectly influence striatal dopamine levels by selectively modulating patch output. Indeed, there is evidence that local enk administration promotes dopamine metabolism in dorsal striatum (Biggio et al., 1978). Such an interaction would provide a route for integration of sensorimotor and limbic signals.

Our results suggest that future studies into the behavioral significance of opioids in dorsal striatum should consider effects via DORs. Due to the clear role of MORs in addiction, most prior studies into opioid signaling in striatum have focused on MORs in the context of behavioral reinforcement (Burkett et al., 2011; Cui et al., 2014; DiFeliceantonio et al., 2012). However, local administration of opioids is not inherently rewarding in dorsal striatum (Bals-Kubik et al., 1993; van der Kooy et al., 1982). Optogenetic stimulation and inhibition of excitatory inputs to dorsomedial patches was recently shown to impact cost-benefit decision making in rats (Friedman et al., 2015). Critically, the influence of stimulation was context dependent. Our data raise the possibility that by sensitizing patch SPNs to excitatory input through disinhibition, opioids could contribute to such decision-making processes by providing a context signal.

In this study, we examined opioid modulation in the dorsal striatum, with the expectation that enk actions through MORs would provide compartment-specificity. Instead, we found only a minor role for MORs, despite their striking abundance in patches, suggesting that the primary role of MORs in patches is not to mediate suppression of inhibition. Indeed, MORs are most prominently localized in SPN dendrites and dendritic spines (Wang et al., 1996). Given the lack of compartment-specific modulation of excitatory transmission and the relatively weak MOR-dependent modulation of inhibition, we speculate that these post-synaptic receptors may play a role in the gating of synaptic plasticity and tuning cellular responses to other neuromodulators such as dopamine.

EXPERIMENTAL PROCEDURES

Mice

Pdyn-EGFP transgenic mice (GENSAT, founder line BD193) (Gong et al., 2003) were crossed with other transgenic mice (as described in the appropriate figure legends) and maintained on a C57BL/6 background. A full list of mouse strains is provided in the Supplemental Experimental Procedures. All

experimental manipulations were performed in accordance with protocols approved by the Harvard Standing Committee on Animal Care following guidelines described in the US NIH *Guide for the Care and Use of Laboratory Animals*.

Stereotaxic Intracranial Injection

Male and female mice (postnatal day 2–9) were anesthetized with isoflurane and placed in a small animal stereotaxic frame (David Kopf Instruments). After puncturing the skin and skull under aseptic conditions, AAVs were injected (0.5–1 μl total volume) bilaterally through a pulled glass pipette at a rate of 100 nl/min using a UMP3 microsyringe pump (World Precision Instruments). Depending on the size of the mouse, injection coordinates ranged between 0 to +0.5 mm from bregma, 0.5 to 1.0 mm lateral, and 1.8 to 2.3 mm below pia for dorsal striatum. After surgical procedures, mice were returned to their home cage for >21 days to allow for maximal gene expression.

Immunohistochemistry

Brain tissue was fixed using 4% paraformaldehyde and processed using standard methods, as described in the Supplemental Experimental Procedures, which also lists all antibodies used. Whole sections were imaged with an Olympus VS110 slide scanning microscope using a 10× objective. Mosaic images were automatically constructed by the microscope's OlyVIA software. For Figures 1B, 2A, and 2B, high-resolution images of regions of interest were subsequently acquired with a Leica SP8 X confocal microscope using a 20× 0.75 NA oil immersion objective (Harvard NeuroDiscovery Center). Images represent maximum intensity projections of 15–25 μm (Figure 1B) or 40–80 μm (Figures 2A and 2B) confocal stacks.

FISH

Mice were deeply anesthetized with isoflurane and decapitated, and their brains were quickly removed and frozen in tissue freezing medium on dry ice. Brains were cut on a cryostat (Leica CM 1950) into 30 μm sections, adhered to SuperFrost Plus slides (VWR), and immediately refrozen. Samples were fixed 4% paraformaldehyde, processed according to ACD RNAscope Fluorescent Multiplex Assay manual, and coverslipped with ProLong antifade reagent (Molecular Probes). Sections were imaged on a Leica SP8 X confocal microscope using a 63× 1.4 NA oil immersion objective (Harvard NeuroDiscovery Center). Tiled z stacks (3–5 μm) were obtained to cover large areas around patches, visually identified by high levels of *Pdyn* signal.

Image Analysis

SPN cell density and EGFP/tdTomato co-localization were determined using confocal images of sections from *Pdyn*-EGFP and *Pdyn*-EGFP;*Drd1a*-tdTomato mice stained with the appropriate antibodies, as described in the Supplemental Experimental Procedures. FISH images were analyzed using a custom macro in Image J, as described in the Supplemental Experimental Procedures.

Acute Brain Slice Preparation

Coronal brain slices (300-μm thick) were obtained from 28- to 35-day-old mice (both male and female) using standard techniques, as described in the Supplemental Experimental Procedures. Briefly, animals were perfused with ACSF, brains were sliced in ice-cold choline-based solution, recovered in at 34°C in ACSF, and subsequently maintained at room temperature (20°C–22°C) until use.

Electrophysiology

Detailed procedures are available in the Supplemental Experimental Procedures. Briefly, slices were placed in a recording chamber mounted on an upright customized microscope (Olympus BX51WI) and continuously superfused (4 ml/min) with ACSF warmed to 31°C–33°C for whole-cell voltage-and current-clamp recordings. Patch pipettes (2–4 MΩ) pulled from borosilicate glass (G150F-3, Warner Instruments) were filled either with ACSF for cell-attached current clamp recordings, a Cs^+-based low Cl^- internal solution or a Cs^+-based high Cl^- internal solution (Figures 6A, S7E, and S7F, only) for whole-cell voltage-clamp recordings, or with a K^+-based low Cl^- internal solution for whole-cell current-clamp recordings. To electrically evoke IPSCs, simulating electrode pipettes were placed nearby the recorded cell (~50–150 μm) within the same compartment, and a brief pulse (0.5 ms, 20–80 μA) was delivered at 20-s intervals. To activate ChR2-expressing cells and axons, light from a 473 nm laser (Optoengine) was focused on the back aperture of the microscope objective to produce wide-field illumination with brief pulses of light (2 ms–2 s duration; 0.2–50 $mW \cdot mm^{-2}$ under the objective, see Supplemental Experimental Procedures) at 20 s intervals.

UV Uncaging

UV uncaging (Figures S7G, S8C, and S8D) was carried out as described in Banghart and Sabatini (2012) (see Supplemental Experimental Procedures). Collimated UV illumination was applied over the entire field of view, which typically covered an entire patch.

Electrophysiological Data Acquisition and Analysis

Membrane currents and potentials were amplified and low-pass filtered at 3 kHz using a Multiclamp 700B amplifier (Molecular Devices), digitized at 10 kHz, and acquired using National Instruments acquisition boards and a custom version of ScanImage written in MATLAB (Mathworks). Electrophysiology and imaging data were analyzed offline using Igor Pro (Wavemetrics), custom MatLab scripts, and ImageJ (NIH). In figures, current-clamp and voltage-clamp traces represent the averaged waveform of 3–5 consecutive acquisitions. Peak amplitudes were calculated by averaging over a 2-ms window around the peak. To determine magnitude of modulation by enk, the peak amplitude of six consecutive IPSC amplitudes were averaged once the IPSC reached a stable plateau (4 to 5 min for enk and DAMGO and 6–8 min for SNC-80). IPSC amplitudes were normalized to baseline averages (six consecutive traces immediately prior to drug application).

Statistical Tests

For electrophysiological recordings with bath applications of drugs, significance of modulation was tested by comparing the IPSC peak amplitudes following drug application to the baseline amplitudes using Wilcoxon's sign-ranked test. In the text, this p value appears with the average normalized IPSC and "n" values for a given condition. Wilcoxon's sign-ranked test was also used to compare IPSC amplitudes induced when stimulating electrode is placed inside or outside the patch (Figure 3). To compare the expression levels of *Pdyn*, *Oprm1*, and *Oprd1* transcripts in each patch or matrix cell, we used the two-sample Kolmogorov-Smirnov test (Figure S6). For all other comparisons between different datasets (both images and electrophysiological data), summary values were reported as mean ± SEM and were compared to each other using the Mann-Whitney U test. For all comparisons, p values smaller than 0.05 were denoted with an asterisk.

SUPPLEMENTAL INFORMATION

Supplemental Information includes eight figures and Supplemental Experimental Procedures and can be found with this article online at http://dx.doi.org/10.1016/j.neuron.2015.11.010.

AUTHOR CONTRIBUTIONS

M.R.B., S.Q.N., and B.L.S. conceived of the study, designed experiments and wrote the paper. M.R.B. and S.Q.N. performed experiments and analyzed data. N.C.W. performed the FISH experiments.

CONFLICTS OF INTEREST

The authors declare no competing financial interests.

ACKNOWLEDGMENTS

The authors thank Terence Lee, Raul Lopez, and Alla Avakova for excellent technical assistance; Victoria Abraira and Charles Gerfen for providing brain tissue for analysis of transgenic mouse lines; and Lai Ding for writing the Image

J macro used for FISH analysis. This work was supported by the Helen Hay Whitney Foundation (M.R.B.), the Charles A. King Trust/Bank of America Co-Trustee (M.R.B.), the National Institute on Drug Abuse (K99DA034648 to M.R.B.), the Canadian Institute of Health Research (S.Q.N.), and the National Institute of Mental Health (RO1MH085418 and R01MH100568 to B.L.S.).

Received: July 14, 2015
Revised: October 9, 2015
Accepted: November 5, 2015
Published: December 3, 2015

REFERENCES

Ade, K.K., Wan, Y., Chen, M., Gloss, B., and Calakos, N. (2011). An Improved BAC Transgenic Fluorescent Reporter Line for Sensitive and Specific Identification of Striatonigral Medium Spiny Neurons. Front. Syst. Neurosci. *5*, 32.

Atwood, B.K., Kupferschmidt, D.A., and Lovinger, D.M. (2014). Opioids induce dissociable forms of long-term depression of excitatory inputs to the dorsal striatum. Nat. Neurosci. *17*, 540–548.

Bals-Kubik, R., Ableitner, A., Herz, A., and Shippenberg, T.S. (1993). Neuroanatomical sites mediating the motivational effects of opioids as mapped by the conditioned place preference paradigm in rats. J. Pharmacol. Exp. Ther. *264*, 489–495.

Banghart, M.R., and Sabatini, B.L. (2012). Photoactivatable neuropeptides for spatiotemporally precise delivery of opioids in neural tissue. Neuron *73*, 249–259.

Besson, M.J., Graybiel, A.M., and Quinn, B. (1990). Co-expression of neuropeptides in the cat's striatum: an immunohistochemical study of substance P, dynorphin B and enkephalin. Neuroscience *39*, 33–58.

Biggio, G., Casu, M., Corda, M., Di Bello, C., and Gessa, G. (1978). Stimulation of dopamine synthesis in caudate nucleus by intrastriatal enkephalins and antagonism by naloxone. Science *200*, 552–554.

Blomeley, C.P., and Bracci, E. (2011). Opioidergic interactions between striatal projection neurons. J. Neurosci. *31*, 13346–13356.

Boyden, E.S., Zhang, F., Bamberg, E., Nagel, G., and Deisseroth, K. (2005). Millisecond-timescale, genetically targeted optical control of neural activity. Nat. Neurosci. *8*, 1263–1268.

Burkett, J.P., Spiegel, L.L., Inoue, K., Murphy, A.Z., and Young, L.J. (2011). Activation of μ-opioid receptors in the dorsal striatum is necessary for adult social attachment in monogamous prairie voles. Neuropsychopharmacology *36*, 2200–2210.

Canales, J.J., and Graybiel, A.M. (2000). A measure of striatal function predicts motor stereotypy. Nat. Neurosci. *3*, 377–383.

Chesselet, M.F., and Graybiel, A.M. (1983). Met-enkephalin-like and dynorphin-like immunoreactivities of the basal ganglia of the cat. Life Sci. *33* (*Suppl 1*), 37–40.

Cowan, R.L., Wilson, C.J., Emson, P.C., and Heizmann, C.W. (1990). Parvalbumin-containing GABAergic interneurons in the rat neostriatum. J. Comp. Neurol. *302*, 197–205.

Crittenden, J.R., and Graybiel, A.M. (2011). Basal Ganglia disorders associated with imbalances in the striatal striosome and matrix compartments. Front. Neuroanat. *5*, 59.

Cui, Y., Ostlund, S.B., James, A.S., Park, C.S., Ge, W., Roberts, K.W., Mittal, N., Murphy, N.P., Cepeda, C., Kieffer, B.L., et al. (2014). Targeted expression of μ-opioid receptors in a subset of striatal direct-pathway neurons restores opiate reward. Nat. Neurosci. *17*, 254–261.

Desban, M., Kemel, M.L., Glowinski, J., and Gauchy, C. (1993). Spatial organization of patch and matrix compartments in the rat striatum. Neuroscience *57*, 661–671.

DiFeliceantonio, A.G., Mabrouk, O.S., Kennedy, R.T., and Berridge, K.C. (2012). Enkephalin surges in dorsal neostriatum as a signal to eat. Curr. Biol. *22*, 1918–1924.

Donoghue, J.P., and Herkenham, M. (1986). Neostriatal projections from individual cortical fields conform to histochemically distinct striatal compartments in the rat. Brain Res. *365*, 397–403.

Fallon, J.H., and Ciofi, P. (1990). Dynorphin-containing neurons. In Handbook of Chemical Neuroanatomy, Vol. 9, Neuropeptides in the CNS, Part II, A. Bjorklund, T. Hokfelt, and M.J. Kuhar, eds. (Elsevier), p. 1.

Filliol, D., Ghozland, S., Chluba, J., Martin, M., Matthes, H.W., Simonin, F., Befort, K., Gavériaux-Ruff, C., Dierich, A., LeMeur, M., et al. (2000). Mice deficient for delta- and mu-opioid receptors exhibit opposing alterations of emotional responses. Nat. Genet. *25*, 195–200.

Friedman, A., Homma, D., Gibb, L.G., Amemori, K., Rubin, S.J., Hood, A.S., Riad, M.H., and Graybiel, A.M. (2015). A Corticostriatal Path Targeting Striosomes Controls Decision-Making under Conflict. Cell *161*, 1320–1333.

Fujiyama, F., Sohn, J., Nakano, T., Furuta, T., Nakamura, K.C., Matsuda, W., and Kaneko, T. (2011). Exclusive and common targets of neostriatofugal projections of rat striosome neurons: a single neuron-tracing study using a viral vector. Eur. J. Neurosci. *33*, 668–677.

Gerfen, C.R. (1984). The neostriatal mosaic: compartmentalization of corticostriatal input and striatonigral output systems. Nature *311*, 461–464.

Gerfen, C.R., and Young, W.S., 3rd (1988). Distribution of striatonigral and striatopallidal peptidergic neurons in both patch and matrix compartments: an in situ hybridization histochemistry and fluorescent retrograde tracing study. Brain Res. *460*, 161–167.

Goldman-Rakic, P.S. (1982). Cytoarchitectonic heterogeneity of the primate neostriatum: subdivision into Island and Matrix cellular compartments. J. Comp. Neurol. *205*, 398–413.

Gong, S., Zheng, C., Doughty, M.L., Losos, K., Didkovsky, N., Schambra, U.B., Nowak, N.J., Joyner, A., Leblanc, G., Hatten, M.E., and Heintz, N. (2003). A gene expression atlas of the central nervous system based on bacterial artificial chromosomes. Nature *425*, 917–925.

Graybiel, A.M., and Chesselet, M.F. (1984). Compartmental distribution of striatal cell bodies expressing [Met]enkephalin-like immunoreactivity. Proc. Natl. Acad. Sci. USA *81*, 7980–7984.

Graybiel, A.M., and Ragsdale, C.W., Jr. (1978). Histochemically distinct compartments in the striatum of human, monkeys, and cat demonstrated by acetylthiocholinesterase staining. Proc. Natl. Acad. Sci. USA *75*, 5723–5726.

Guttenberg, N.D., Klop, H., Minami, M., Satoh, M., and Voorn, P. (1996). Co-localization of mu opioid receptor is greater with dynorphin than enkephalin in rat striatum. Neuroreport *7*, 2119–2124.

Herkenham, M., and Pert, C.B. (1981). Mosaic distribution of opiate receptors, parafascicular projections and acetylcholinesterase in rat striatum. Nature *291*, 415–418.

Jiang, Z.G., and North, R.A. (1992). Pre- and postsynaptic inhibition by opioids in rat striatum. J. Neurosci. *12*, 356–361.

Kawaguchi, Y., Wilson, C.J., and Emson, P.C. (1989). Intracellular recording of identified neostriatal patch and matrix spiny cells in a slice preparation preserving cortical inputs. J. Neurophysiol. *62*, 1052–1068.

Khachaturian, H., Lewis, M.E., Tsao, K., and Watson, S.J. (1985). Beta-endorphin, alpha MSH, ACTH, and related peptides. In Handbook of Chemical Neuroanatomy, Vol. 4, GABA and Neuropeptides in the CNS, Part I, A. Bjorklund and T. Hokfelt, eds. (Elsevier), pp. 216–272.

Knapp, R.J., Santoro, G., De Leon, I.A., Lee, K.B., Edsall, S.A., Waite, S., Malatynska, E., Varga, E., Calderon, S.N., Rice, K.C., et al. (1996). Structure-activity relationships for SNC80 and related compounds at cloned human delta and mu opioid receptors. J. Pharmacol. Exp. Ther. *277*, 1284–1291.

Koshimizu, Y., Wu, S.-X., Unzai, T., Hioki, H., Sonomura, T., Nakamura, K.C., Fujiyama, F., and Kaneko, T. (2008). Paucity of enkephalin production in neostriatal striosomal neurons: analysis with preproenkephalin-green fluorescent protein transgenic mice. Eur. J. Neurosci. *28*, 2053–2064.

Kubota, Y., and Kawaguchi, Y. (1993). Spatial distributions of chemically identified intrinsic neurons in relation to patch and matrix compartments of rat neostriatum. J. Comp. Neurol. *332*, 499–513.

Lawhorn, C., Smith, D.M., and Brown, L.L. (2009). Partial ablation of mu-opioid receptor rich striosomes produces deficits on a motor-skill learning task. Neuroscience *163*, 109–119.

Lindskog, M., Svenningsson, P., Fredholm, B., Greengard, P., and Fisone, G. (1999). Mu- and delta-opioid receptor agonists inhibit DARPP-32 phosphorylation in distinct populations of striatal projection neurons. Eur. J. Neurosci. *11*, 2182–2186.

Matthes, H.W., Maldonado, R., Simonin, F., Valverde, O., Slowe, S., Kitchen, I., Befort, K., Dierich, A., Le Meur, M., Dollé, P., et al. (1996). Loss of morphine-induced analgesia, reward effect and withdrawal symptoms in mice lacking the mu-opioid-receptor gene. Nature *383*, 819–823.

Miura, M., Saino-Saito, S., Masuda, M., Kobayashi, K., and Aosaki, T. (2007). Compartment-specific modulation of GABAergic synaptic transmission by mu-opioid receptor in the mouse striatum with green fluorescent protein-expressing dopamine islands. J. Neurosci. *27*, 9721–9728.

Noble, F., and Cox, B.M. (1995). Differential regulation of D1 dopamine receptor- and of A2a adenosine receptor-stimulated adenylyl cyclase by mu-, delta 1-, and delta 2-opioid agonists in rat caudate putamen. J. Neurochem. *65*, 125–133.

Oude Ophuis, R.J.A., Boender, A.J., van Rozen, A.J., and Adan, R.A.H. (2014). Cannabinoid, melanocortin and opioid receptor expression on DRD1 and DRD2 subpopulations in rat striatum. Front. Neuroanat. *8*, 14.

Pennock, R.L., and Hentges, S.T. (2014). Direct inhibition of hypothalamic proopiomelanocortin neurons by dynorphin A is mediated by the μ-opioid receptor. J. Physiol. *592*, 4247–4256.

Penny, G.R., Wilson, C.J., and Kitai, S.T. (1988). Relationship of the axonal and dendritic geometry of spiny projection neurons to the compartmental organization of the neostriatum. J. Comp. Neurol. *269*, 275–289.

Pert, C.B., Kuhar, M.J., and Snyder, S.H. (1976). Opiate receptor: autoradiographic localization in rat brain. Proc. Natl. Acad. Sci. USA *73*, 3729–3733.

Ponterio, G., Tassone, A., Sciamanna, G., Riahi, E., Vanni, V., Bonsi, P., and Pisani, A. (2013). Powerful inhibitory action of mu opioid receptors (MOR) on cholinergic interneuron excitability in the dorsal striatum. Neuropharmacology *75*, 78–85.

Pradhan, A.A.A., and Clarke, P.B.S. (2005). Comparison between delta-opioid receptor functional response and autoradiographic labeling in rat brain and spinal cord. J. Comp. Neurol. *481*, 416–426.

Ragsdale, C.W., Jr., and Graybiel, A.M. (1981). The fronto-striatal projection in the cat and monkey and its relationship to inhomogeneities established by acetylcholinesterase histochemistry. Brain Res. *208*, 259–266.

Reiner, A. (2010). The Conservative Evolutin of the Vertebrate Basal Ganglia. In Handbook of Basal Ganglia Structure and Function, H. Steiner and K.Y. Tseng, eds. (Academic Press), pp. 29–62.

Reiner, A., Medina, L., and Veenman, C.L. (1998). Structural and functional evolution of the basal ganglia in vertebrates. Brain Res. Brain Res. Rev. *28*, 235–285.

Rushlow, W., Naus, C.C., and Flumerfelt, B.A. (1996). Somatostatin and the patch/matrix compartments of the rat caudate-putamen. J. Comp. Neurol. *364*, 184–190.

Stephenson-Jones, M., Ericsson, J., Robertson, B., and Grillner, S. (2012). Evolution of the basal ganglia: dual-output pathways conserved throughout vertebrate phylogeny. J. Comp. Neurol. *520*, 2957–2973.

Tajima, K., and Fukuda, T. (2013). Region-specific diversity of striosomes in the mouse striatum revealed by the differential immunoreactivities for mu-opioid receptor, substance P, and enkephalin. Neuroscience *241*, 215–228.

Toll, L., Berzetei-Gurske, I.P., Polgar, W.E., Brandt, S.R., Adapa, I.D., Rodriguez, L., Schwartz, R.W., Haggart, D., O'Brien, A., White, A., et al. (1998). Standard binding and functional assays related to medications development division testing for potential cocaine and opiate narcotic treatment medications. NIDA Res. Monogr. *178*, 440–466.

van der Kooy, D., Mucha, R.F., O'Shaughnessy, M., and Bucenieks, P. (1982). Reinforcing effects of brain microinjections of morphine revealed by conditioned place preference. Brain Res. *243*, 107–117.

Wang, H., Moriwaki, A., Wang, J.B., Uhl, G.R., and Pickel, V.M. (1996). Ultrastructural immunocytochemical localization of mu opioid receptors and Leu5-enkephalin in the patch compartment of the rat caudate-putamen nucleus. J. Comp. Neurol. *375*, 659–674.

Watabe-Uchida, M., Zhu, L., Ogawa, S.K., Vamanrao, A., and Uchida, N. (2012). Whole-brain mapping of direct inputs to midbrain dopamine neurons. Neuron *74*, 858–873.

White, N.M., and Hiroi, N. (1998). Preferential localization of self-stimulation sites in striosomes/patches in the rat striatum. Proc. Natl. Acad. Sci. USA *95*, 6486–6491.

Zhang, S., Tong, Y., Tian, M., Dehaven, R.N., Cortesburgos, L., Mansson, E., Simonin, F., Kieffer, B., and Yu, L. (1998). Dynorphin A as a potential endogenous ligand for four members of the opioid receptor gene family. J. Pharmacol. Exp. Ther. *286*, 136–141.